Robust measurement of microbial reduction of graphene oxide nanoparticles using image analysis

Danielle T. Bennett, Anne S. Meyer#

Department of Biology, University of Rochester, Rochester, New York, United States

Running Head: Image Analysis of Microbial Graphene Oxide Reduction

Address correspondence to Anne S. Meyer, anne@annemeyerlab.org.

ABSTRACT

Shewanella oneidensis (*S. oneidensis*) has the capacity to reduce electron acceptors within a medium and is thus used frequently in microbial fuel generation, pollutant breakdown, and nanoparticle fabrication. Microbial fuel setups, however, often require costly or labor-intensive components, thus making optimization of their performance onerous. For rapid optimization of setup conditions, a model reduction assay can be employed to allow simultaneous, large-scale experiments at lower cost and effort. Since *S. oneidensis* uses different extracellular electron transfer pathways depending on the electron acceptor, it is essential to use a reduction assay that mirrors the pathways employed in the microbial fuel system. For microbial fuel setups that use nanoparticles to stimulate electron transfer, reduction of graphene oxide provides a more accurate model than other commonly used assays as it is a bulk material that forms flocculates in solutions with a large ionic component. However, graphene oxide flocculates can interfere with traditional absorbance-based measurement techniques. This study introduces a novel image analysis method for quantifying graphene oxide reduction, showing improved performance and statistical accuracy over traditional methods. A comparative analysis shows that the image analysis method produces smaller errors between replicates and reveals more statistically significant differences between samples than traditional plate reader measurements under conditions causing graphene oxide flocculation. Image analysis can also detect reduction activity at earlier time points due to its utilization of larger solution volumes, enhancing color detection. These improvements in accuracy make image analysis a promising method for optimizing microbial fuel cells that use nanoparticles or bulk substrates.

IMPORTANCE

Shewanella oneidensis (*S. oneidensis*) is widely used in reduction processes such as microbial fuel generation due to its capacity to reduce electron acceptors. Often, these setups are labour

intensive to operate and require days to produce results, so use of a model assay would reduce the time and expense needed for optimization. Our research developed a novel digital analysis method for analysis of graphene oxide flocculates that may be utilized as a model assay for reduction platforms featuring nanoparticles. Use of this model reduction assay will enable rapid optimization and drive improvements in the microbial fuel generation sector.

INTRODUCTION

Shewanella oneidensis is a bacterium that can drive microbial fuel generation[1–5], breakdown of azo dye pollutants[6–8], and fabrication of nanoparticles[2] due to its capacity for transferring electrons to electron acceptors within a medium[2,7,9–11]. Natively, this electron transferral facilitates bacterial respiration using extracellular electron acceptors like Fe(III)[12]. Electron transfer by the *S. oneidensis* organism is accomplished through several alternative routes intercellularly and extracellularly, including electron shuttling by flavin secretion[13–16], through nanowire structures produced by the bacterium[10,17,18], or through direct membrane pathways[19,20]. Flavins are soluble shuttle molecules which are released by the bacteria into solution[21]. In both the nanowire and the direct membrane pathways, metal reduction has been largely attributed to a set of surface Mtr/Omc proteins[22,23] that includes three outer membrane decaheme c-type cytochromes (MtrC, MtrF, OmcA), two periplasmic decaheme cytochromes (MtrA and MtrD), and two outer membrane non-cytochrome proteins (MtrB, MtrE)[22–26]. These proteins funnel electrons to cytochromes embedded in the outer membrane of the bacterium, allowing extracellular electron transfer in particular for metallic iron electron acceptors[3,24,27]. This capacity also enables use of this organism to reduce a wide range of extracellular electron acceptors[11], including desalination of salt water[6–8,28] , bioremediation of pollutants in soil[28] and powering environmental sensors[4,29].

Since microbial fuel cell setups can be complex and require extended time periods to produce results[4,28], efficiency of the fuel cells may be improved using a model reduction assay to quickly test new reaction conditions. The reduction of the acceptor in microbial fuel cells may proceed through any of the *S. oneidensis* electron transfer pathways, and the specific reduction pathway that is utilized by the bacterium varies in different circumstances[16,30,31]. Flavin pathways seem to dominate in systems with insoluble electron acceptors and under certain ratios of electron donors and acceptors[16,30,31], nanowire pathways seem to dominate when the organism is under stress due to nutrient deficiency[3,10,18,32], and Mtr pathways are important in anaerobic conditions[33–35]. The dominant pathway can also depend on the type of electron acceptor present in the extracellular environment[21,36,37]. Thus, to improve the efficiency of microbial fuel-generating setups utilizing a model reduction assay, the model reduction assay must utilize the same reduction pathway as the fuel cell.

Model assays to monitor *S. oneidensis* reduction frequently involve observing the variation in absorbance over time as dye compounds such as methylene blue[13,38] or Congo red[13] are reduced and become colorless. Another common assay, the ferrozine assay, creates conditions of excess iron under which an iron transport pathway termed FoeE is particularly important in reduction[39]. The ferrozine assay is representative of reduction pathways involving soluble metal ions in solution or media with excess iron[39], while Congo red reduction features soluble electron acceptors, particularly those which utilize the Mtr pathway with dependence on the CymA cytochrome[13]. For insoluble electron acceptors such as nanoparticles or bulk conductive solids, these assays will not be appropriately representative. Instead, a graphene oxide reduction assay is more suitable since graphene oxide forms insoluble nanoparticle flocculates in solution with sizes ranging from 1 nm in diameter in colloidal solution to 20 µm in acidic or high-concentration conditions[40,41]. Graphene oxide reduction by *S. oneidensis* has been shown to require the Mtr respiratory pathway[15] with particular dependence on MtrF and CymA[42]. This

reduction process is also enhanced by electron shuttling pathways, which are more prominent when the electron acceptor is a bulk substrate[15]. Graphene oxide reduction reactions can be performed under conditions that cause the graphene oxide to flocculate, a type of aggregation, which can take place in solution under certain pH and concentration conditions[40]. *S. oneidensis* reduction of graphene oxide flocculates may thus serve as a model assay for systems that reduce nanoparticles or bulk substrate. Graphene oxide flocculates form rapidly[40,43] and do not require the technical complexity of nanoparticle synthesis[23], making them well-suited for use as a model system of a microbial fuel cell that features nanoparticles. However, monitoring the absorbance of graphene oxide using traditional spectroscopic methods is challenging due to this flocculation, which causes increased error in readings due to drift of the large particles. Visually, reduction of graphene oxide produces a color change from light brown to dark black as the graphene oxide is reduced[23], and this visual color difference may be used to measure directly the transfer of electrons to bulk substrate or nanoparticle electron acceptors. Hence there is an opportunity for image analysis of graphene oxide reduction to provide quantitative information on the extent of reduction of the graphene oxide over time.

Image analysis methods are commonly used in nanoparticle sensing[44,45], in which images of the samples are analyzed for the average 'color' of each. Color is interpreted using a set of three vectors known as a 'color space'[46] such as RGB (red, green, and blue) which contains the corresponding percentage of 'red', 'green,' or 'blue' for each pixel. For images that include fluctuating lighting or reflections, the HSV color space (hue, saturation, and value) is more robust due to the separation of lighting information into the saturation and value vectors[46–48]. By averaging the HSV vectors of a region of interest of an image of a graphene oxide sample over time, the reduction of graphene oxide over time by *S. oneidensis* may be measured. This method is advantageous for monitoring graphene oxide solutions that have flocculates present because the averaging is performed over a larger area of the sample, thereby avoiding

confounding effects from the flocculates settling within the solution. This new method of combining image analysis techniques with an unconventional graphene oxide reduction assay will enable model assays for microbial fuel cells featuring bulk substrate and nanoparticles.

RESULTS

Determination of the average Hue, Saturation and Value vectors for images of graphene oxide.

Custom Matlab™ code was written to determine the hue (H), saturation (S) and value (S) vector distribution across images of graphene oxide solutions (Figure 1A). Images of experimental samples were cropped to obtain a rectangular region of interest containing glare or reflection. Points were then selected in regions with no glare or reflections (Figure 1B). Selection of 15 points or more was found to reduce the standard error of all selected points across each image to 0.09 % or less of the vector value on average (Supplemental Figure 1). A 32 x 32 pixel box was selected around each point (Figure 1C), and the average value of each pixel within the box was calculated to obtain the average hue, saturation, and value vectors for each region of interest selected.

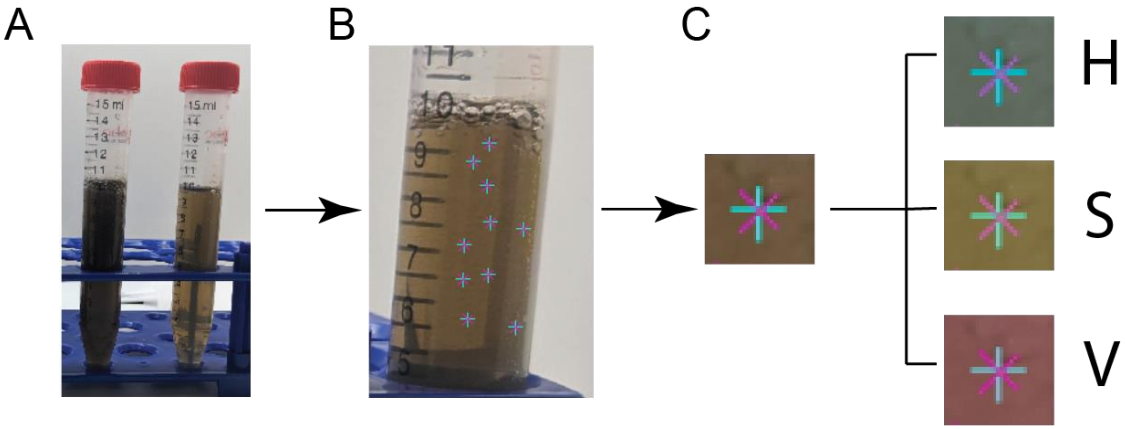

Figure 1: The workflow of the value vector analysis. A) A region of the image was selected that contains the least interference from the background of the sample. B) At least 12 points

were selected that did not contain interference from tube labels or reflections. C) For each selected point, a 32 x 32 pixel box was cropped around the point, and the image information was separated into three vectors: hue (H), saturation (S) and value (V). The value vector contains information about the brightness or darkness of the image, represented as a number between 0 and 1, where 0 is the darkest and 1 is the lightest. The value vector was averaged over all the selected pixels to obtain an average value for each box. All boxes were then averaged to obtain an overall average value for each sample. This overall averaged value was used as a representation of the extent of graphene oxide reduction.

Correlation between average HSV value and graphene oxide concentration

To determine the suitability of image analysis for measuring graphene oxide reduction, experiments were performed to determine whether HSV value correlated with graphene oxide concentration. Different concentrations of graphene oxide were prepared, and image analysis values for the hue, saturation, and value vectors were measured (Figure 1).

The hue and saturation vectors did not vary linearly with increasing graphene oxide concentration, rather reaching a binary saturation point (Supplemental Figure 2). However, the value vector, which is representative of the brightness of an image[48], demonstrated linear behaviour as a function of the graphene oxide concentration in some regions of the data (Figure 2). At lower concentrations of graphene oxide, increasing the graphene oxide concentration resulted in decreasing average HSV value of the samples. The average HSV value of the samples plateaued at graphene oxide concentrations around 40 %, or 0.40 g/L. Lower concentrations of graphene oxide between 6 – 12 % were used for future experiments in order to utilize a range over which the image analysis will be sensitive. These results demonstrated that the average HSV value measurement, as opposed to the hue or saturation, showed the

closest correlation with increasing graphene oxide concentration and that this measurement approach could be a promising technique for monitoring graphene oxide reduction over time.

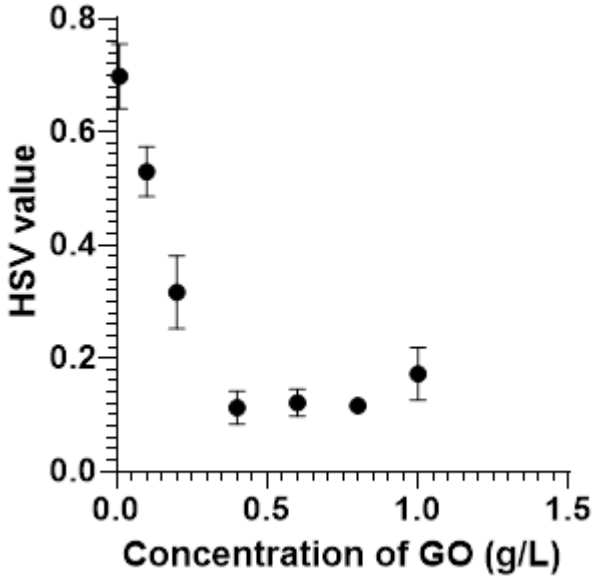

Figure 2: The average calculated HSV value vectors of samples with concentrations of graphene oxide varying from 0.01 – 1 g/L. Triplicate measurements were taken for each sample, and the results were averaged. The error was the standard deviation of these triplicate measurements.

Image analysis provides more sensitive measurements of graphene oxide reduction by *S. oneidensis* than plate reader absorbance measurements

Since plate reader absorbance measurements are the current standard for measuring bacterial graphene oxide reduction, experiments were performed to compare the accuracy and sensitivity of the image analysis method with plate reader absorbance measurements. A solution of graphene oxide was reduced by *S. oneidensis* bacteria either with or without lactic acid as an electron donor. For this experiment, aliquots were taken from each sample at specific time points and used for plate reader analysis (Figure 3A) as well as imaging the samples, allowing for the two analysis techniques to be directly compared (Figure 3B). The lack of electron donor present in the samples with 0 mM lactic acid was expected to result in minimal bacterial

reduction rates, and thus determining the level of difference between samples with and without

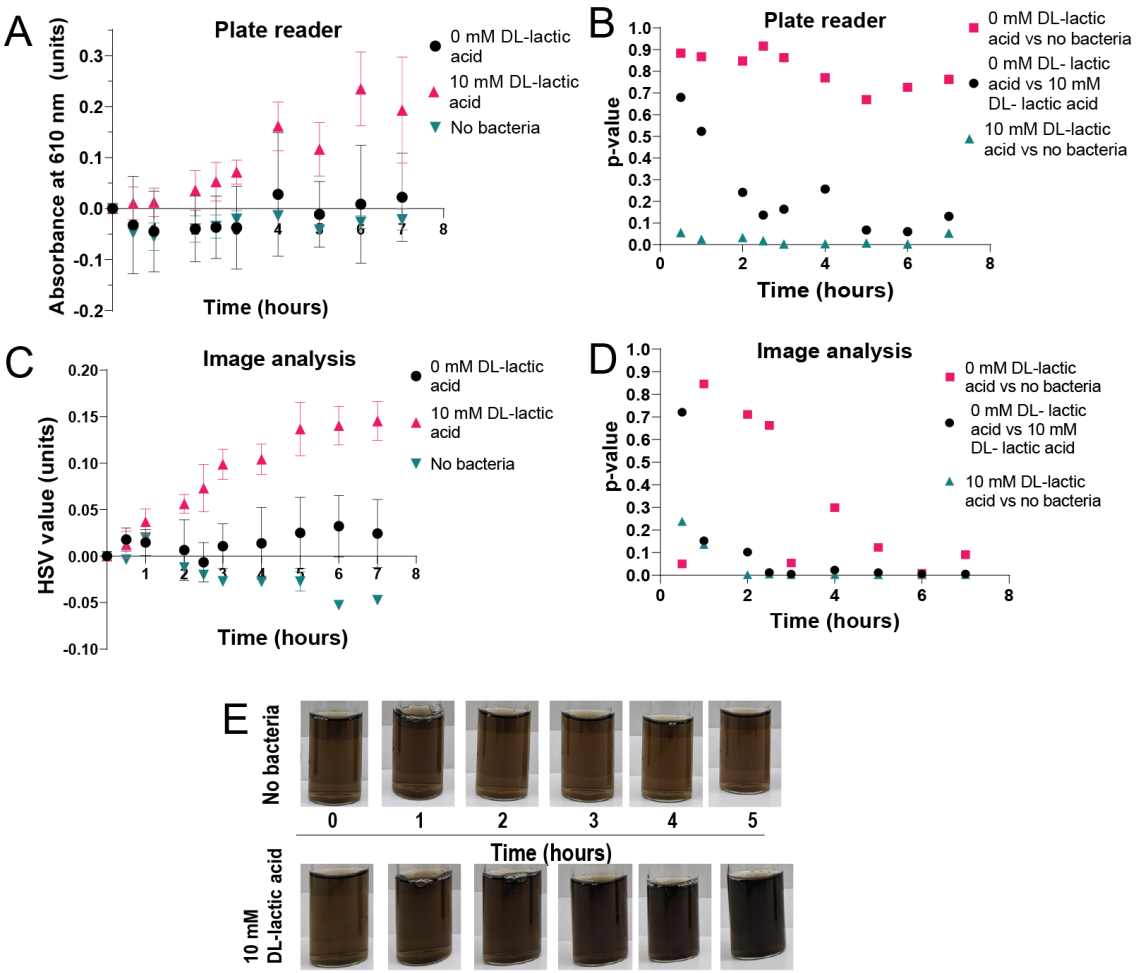

Figure 3: Comparison of plate reader and image analysis of bacterial graphene oxide reduction. A) Analysis of the reduction of graphene oxide by *S. oneidensis* over time by plate reader measurements of the absorbance of a 100 µL aliquot at 610 nm. The statistical difference between samples was calculated to have a p value = 0.0007, with an W ratio of 9.046 (3.000, 17.71). B) Bootstrapping statistical analysis of the p-value of different sample comparisons for the plate reader data at different timepoints. C) Image analysis measurements of the same samples, resulting in an averaged HSV value representation of the graphene oxide reduction. The statistical significance of the difference between samples was calculated to have a p-value < 0.0001 with an W ratio of 20.06 (3.000, 17.67). The errors represent the standard deviation of triplicate repeats of each sample. D) Bootstrapping statistical analysis of the p-value of different sample comparisons for the image analysis data at different timepoints. E) Images of a single sample of graphene oxide with no bacteria (top) or 10 mM lactic acid as an electron source (bottom) over time. Samples with no bacteria were used as a control to detect background levels of graphene oxide reduction. The samples with 0 mM lactic acid and with 10 mM lactic acid both contained identical initial concentrations of bacteria. The statistical significance of the difference between samples was calculated using one way ANOVA with a Welch's correction as well as bootstrapping analysis.

lactic acid will allow for comparing the sensitivity of each analysis technique. For these results,

initial measurements were subtracted from subsequent measurements to normalize for variation in graphene oxide amounts between samples and allow for comparison between two techniques with different y axis units. Any negative values for the samples were assumed to be due to random fluctuation of the measurement paired with this subtraction. Plate reader absorbance measurements of timed aliquot extractions were taken at 610 nm in a 96 well plate, and at this same time-point the samples were imaged to provide a direct comparison with the image analysis.

The plate reader measurements showed an increase in average absorption over time after an initial lag phase for the samples containing lactic acid, indicating reduction of the graphene oxide (Figure 3A). Minimal changes in absorption were measured for the samples without lactic acid or without bacteria. The image analysis results also showed an increase in average HSV value over time for the samples containing lactic acid, though the apparent lag phase was shorter (Figure 3C). The no-lactic-acid and no-bacteria control samples again showed minimal changes in absorption. The limit of detection of a sensing assay may be estimated by obtaining the overall mean of a control sample and then adding three standard deviations to obtain an upward estimate[49,50]. To compare the different techniques, this limit of detection was normalised by the highest detected value of the assay. The normalised value was 0.07 units for the plate reader and 0.29 units for the image analysis. This result shows that the limit of detection of the plate reader assay was lower than that of the image analysis and thus the plate reader is more sensitive. However, the lower W ratio (analogous to the F statistic[51]) for the plate reader analysis measurements indicates that the statistical difference between the samples with 10 mM lactic acid, without lactic acid, and without bacteria is lower for the plate reader measurements than for the image analysis data[51]. This result indicates that there is improved statistical separation between different sample types for the image analysis data.

To further investigate the statistical differences between sample types, bootstrapping analysis was performed on both datasets to provide an improved p-value analysis for small datasets at different time points[52]. For the plate reader analysis method (Figure 3.B), the p-value did not reach a confidence interval of 95 % for the comparison of the sample with 0 mM lactic acid and the sample with no bacteria, so these groups were not significantly different. The comparison between the plate reader samples with 0 mM lactic acid and 10 mM lactic acid revealed that a 95 % confidence interval was reached after 5 hours. This result indicates that these groups became statistically significantly different at the 5-hour timepoint. The plate reader sample containing 10 mM lactic acid and the sample with no bacteria were significantly statistically different throughout the experiment. In contrast, bootstrapping analysis of the image analysis method (Figure 3.D) indicated that the sample with 0 mM lactic acid and the sample with no bacteria reached statistically significant separation after 6 hours, and the 0 mM lactic acid sample and the 10 mM lactic acid sample reached statistically significant separation earlier at 2.25 hours. The sample with 10 mM lactic acid and the control sample with no bacteria became significantly statistically different at 2 hours. Since the three groups were expected to have a large difference in the rate of extra-cellular reduction for graphene oxide, reaching significant statistical separation at earlier timepoints indicates improved precision of the image analysis technique.

Visual comparison of the vials of two different samples over time, with one containing no bacteria and one with 10 mM lactic acid added as an electron donor, showed a qualitative difference at the two-hour time point, with the 10 mM lactic acid sample appearing darker (Figure 3E). This difference was reflected in the image analysis data but not the plate reader measurements. Reduction was indicated by the separation between the control and samples with lactic acid. The image analysis data trendline (Figure 3C) also plateaus around the five-hour time point, whereas the plate reader data does not show a clear plateau (Figure 3A). For

bacterial reduction, a Gompertz trendline exhibiting a lag period, a period of exponential growth and then a plateau is expected[53,54]. This fit is often used for bacterial growth curve fitting[53,55] and is applicable for bacterial consumption of analytes[53]. The plateau in the image analysis data trendline (Figure 3C) could indicate expected Gompertz reduction activity, or it could indicate that the sensor was saturated. The clear plateau for the image analysis method that is not present for the plate reader analysis method is indicative of the higher precision of the image analysis technique.

Influence of differing initial bacterial densities on measurements of graphene oxide reduction by *S. oneidensis*

Since bacterial cells[56] and reduced graphene oxide[57] can have overlapping optical density absorbance peaks, techniques to measure graphene oxide reduction can potentially be confounded by the density of bacteria cells in the samples. Experiments were thus performed to examine the impact of differing initial $O.D._{600}$ densities of bacteria on both the plate reader and image analysis techniques for measuring bacteria graphene oxide reduction. To avoid a plateau from analyte consumption and improve bacterial growth, electron donors were provided in excess via lysogeny broth. Providing too much excess lactic acid in combination with the high ion concentrations of the Minimal media causes near-instantaneous flocculation of graphene oxide into large flakes that settle too fast for imaging[40]. To circumvent this issue, lysogeny broth was used to provide electron donors. *S. oneidensis* bacteria were added at initial $O.D._{600}$ densities ranging from 0.02 to 0.3. Timepoint aliquots were analysed by the plate reader and image analysis for direct comparison as outlined previously (Figure 4).

The plate reader measurement data (Figure 4A) showed a trend of higher absorbance values for samples of higher initial starting $O.D._{600}$, with the $O.D._{600}$ of samples containing bacteria showing significantly higher absorbance than the control sample without bacteria (W statistic

of 10.06 (5.000, 15.57) with a p value of 0.0002). The samples with differential $O.D._{600}$ were not statistically different overall (W statistic of 1.000 (4.000, 15.56) and a p value of 0.4368). Using a paired T-test, the sample with $O.D._{600}$ 0.3 was statistically different to $O.D._{600}$ 0.16 (p value of 0.049). The image analysis data (Figure 4B) showed statistically significant differences between the control sample with no bacteria and the samples containing bacteria (W statistic of 17.17 (5.000, 15.91) with a p value < 0.0001). The samples with differential $O.D._{600}$ were not significantly statistically different (W statistic of 0.2444 (4.000, 16.25) with a p value of 0.909). Paired T-test analysis did not reveal significant differences between any of the individual bacteria-containing samples for the plate reader assay. The plate reader measurement data (Figure 4A) showed linear trendlines for the samples containing bacteria

whereas the image analysis data for the samples containing bacteria (Figure 4B) had a slight plateau.

Both analysis techniques showed significant statistical difference between the samples containing bacteria and the control sample without, but the image analysis technique had a

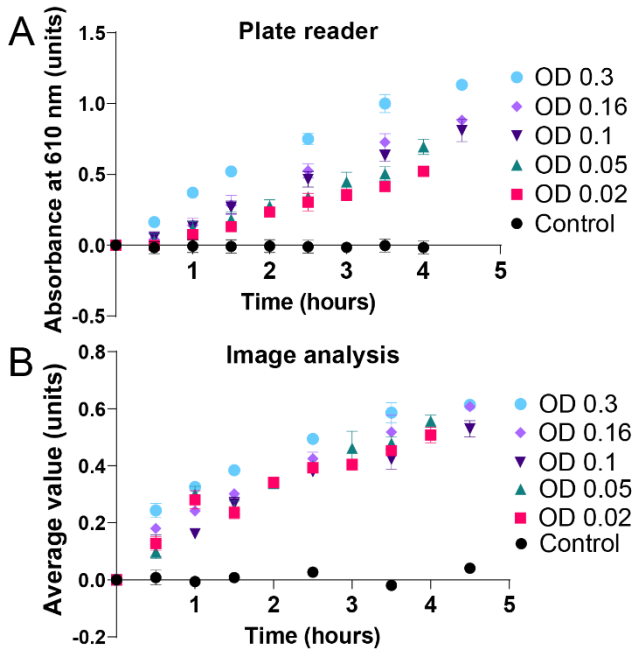

Figure 4: A. Plate reader measurements and B. image analysis of graphene oxide samples containing different starting O.D.$_{600}$ of *S. oneidensis*. Each sample was measured in triplicate, and the errors are representative of the standard deviation of these triplicate measurements. Some errors were too small to visualize on the graph. The control samples contained no bacteria. The statistical significance of the difference between sample sets was calculated using one way ANOVA with a Welch's correction. For comparison of samples with the control sample, the W statistic for the plate reader data was 10.06 (5.000,15.57) with a p value < 0.0002. The W statistic for the image analysis data was 17.17 (5.000, 15.91) with a p value < 0.0001.

lower p value than the plate reader analysis (0.0002 and < 0.0001 respectively). This result again indicates increased precision of the image analysis technique. The differences between the sample with O.D.$_{600}$ 0.3 and the sample with O.D.$_{600}$ 0.16 that were present only in the plate reader analysis could potentially be due to increased sensitivity of the plate reader. However, the p value of this measurement was very close to 0.05 and was not highly statistically significant. An alternative explanation for the difference seen between samples containing

varying starting bacterial densities in the plate reader measurements is that the ability of this assay to measure graphene oxide reduction can be confounded by bacterial density.

DISCUSSION

Graphene oxide reduction assays are promising candidates for application as a model assay for *S. oneidensis* reduction platforms featuring nanoparticles, since the flocculates formed by the graphene oxide would imitate nanoparticle electron acceptors[15,23]. Such a model assay would enable quick optimization of the microbial reduction platform with less resource expense. However, tailoring the electron receiver to match the original platform is important since *S. oneidensis* has multiple reduction pathways, and the dominant pathway is influenced by media composition[30] or the specific electron acceptor[6,19,30,58]. Graphene oxide is well-suited for this purpose, but measuring the progression of the reduction reaction accurately via absorbance assays is difficult due to the flocculates. In this study, we compared traditional absorbance measurements utilizing a microwell plate reader as the gold standard[59] with a novel digital image analysis method for a *S. oneidensis* extracellular reduction assay featuring graphene oxide flocculates[23]. The digital analysis was first optimized by determining which vector from the HSV color space would correlate most closely with graphene oxide concentration, guided by the hypothesis that correlation between an HSV vector and the graphene oxide concentration increase, which also causes similar darkening of the sample, would be representative of the color change caused by graphene oxide reduction. The HSV value vector varied linearly with increased graphene oxide within a defined range of concentrations (Figure 2), unlike the hue and saturation vectors (SI Figure 1). Hue has a sharp cut off when the colour was majority black and is thus unsuitable for monitoring gradual changes over time. Saturation was seemingly uncorrelated with the concentration of graphene oxide and was thus unsuitable. The value vector decreases with increasing graphene oxide concentration and plateaus, making it the best candidate for monitoring graphene oxide concentration using image analysis. From

this data, it was hypothesized that the HSV value vector could be utilized via image analysis to be representative of graphene oxide reduction within a solution due to bacterial reduction, producing measurements varying from 0 (lightest) to 1 (darkest).

The image analysis technique was then used to measure a samples in a bacterial graphene oxide reduction assay, and these data were compared to measurements taken by a plate reader, currently the most standard method for quantifying bacterial reduction assays[59]. Analysis measurements were compared for samples containing differential levels of lactic acid as an electron donor for the *S. oneidensis*. The guiding hypothesis of this experimental set was that the samples with no electron donor would have slow extracellular reduction compared to those with electron donor present[23,60,61] since *S. oneidensis* consumes lactic acid as an electron donor and transfers the electrons extra-cellularly to the graphene oxide flocculates[30,37,62]. *S. oneidensis* will eventually use the acetate it produces as a waste product as an electron source, but this reaction proceeds relatively slowly[14,63]. Thus, the statistical differences between samples would provide a measurement of the sensitivity and accuracy of the analysis method. The graphene oxide in the control solutions with no bacteria became lighter over time (Figure 3) which could be due to some larger flocculates being degraded by the shaking conditions of the experiment[64].

Image analysis measurements (Figure 3A) showed larger differences between experimental and control samples and smaller error bars when compared to the plate reader measurements for these bacterial graphene oxide reduction experiments (Figure 3B). This increased error was likely due to two main challenges with absorbance measurements of the graphene oxide assay. Firstly, graphene oxide can form nanoparticle-like flocculates, particularly under acidic conditions[40] and can be formed into small nanoparticles by *S. oneidensis*[23]. These flocculates settle to the bottom of the 96 microwell plate over time, which will affect the reading taken by the plate reader by variably obstructing the light source. The image analysis method can select

small sections of the flakes themselves and analyse the color – and hence was not dependent on light translation through a sample. Secondly, graphene oxide absorption is usually monitored by observing the shift in the absorbance maximum from 226 nm to 262 nm for reduced graphene oxide[57]. However, due to the presence of UV-active components in the minimal media and the bacteria themselves, the intensity of this peak will be obfuscated by the other components of the media. Instead, a broad absorbance peak centred around 610 nm can be used for monitoring the reduction of graphene oxide[65]. The 610 nm absorption peak of the reduced graphene oxide also overlaps with the absorption peak of the bacteria, usually measured at 600 nm[66]. The image analysis does not encounter this challenge as it is not measuring absorption of a wavelength value but visual color change. The larger area of analysis employed for the image analysis method also reduces the impact of the flocculates. The image analysis measurements showed increased statistically significant differences between different sample types, less overlap of error bars, and the trendline contained a lag phase and a plateau consistent with the Gompertz growth expected from microbial reduction[53] compared to the corresponding the plate reader measurements (Figure 3B). As the three samples groups are expected to have a large difference in the extra-cellular reduction of graphene oxide, this improved separation suggests improved sensitivity of the image analysis technique.

A plateau in graphene oxide reduction was expected to be observed at later time points of the bacteria reduction assays when the bacteria have reached high cell densities or consumed all lactate present within the sample[67]. Consumption of lactate by *S. oneidensis* has been reported at a rate of 11.8 mM/hour at high concentration of bacteria ($O.D._{600}$ ~ 0.2)[61]. The plateau observed by the image analysis at the five-hour time point for reduction samples containing 10 mM of lactic acid was therefore expected (Figure 3A). However, the plateau could also be due to earlier saturation of the image analysis measurement due to larger volumes of analysis. This is unlikely as further experiments obtained a Value vector maximum of 0.55 units, compared

to the plateau maximum of 0.15 units from this experiment. The lack of plateau for the plate reader measurements could be due to decreased resolution of the method or increased range of measurement. Overall, the image analysis data offered high resolution compared to the greater sensitivity of the plate reader analysis method. As *S. oneidensis* is frequently used for bioreactor research, information on the rate of reduction over time is important for improving the efficiency of such systems[60,62] so higher resolution resulting in earlier detection of reduction using the digital analysis is advantageous.

Following the promising results of these experiments, the impact of the initial optical density of bacteria on both the plate reader and image analysis measurement techniques was investigated. This experiment was designed to determine whether the overlapping optical density absorbance peak of the bacteria with that of the graphene oxide would cause erroneous measurements of graphene oxide reduction in conditions with higher bacterial density. To aid the bacterial growth in this experiment, electron donors and nutrients were provided in excess. For the plate reader measurement data, the sample with the highest initial bacteria $O.D._{600}$ was statistically different compared to the samples with lower bacteria densities, while for the image analysis measurement data the only significant differences were between the samples containing no bacteria and those with bacteria. Increased reduction rates with increased concentration of bacteria was not necessarily expected[68] as *S. oneidensis* slows its electron transfer during log phase growth[69]. The differences seen for the plate reader sample with the highest initial $O.D_{600}$ were then likely caused by interference from the spectral overlap between the bacterial absorbance and the reduced graphene oxide absorbance measurement at 600 nm. The lack of this effect in the image analysis measurements demonstrates its effectiveness of this method in a range of different experimental conditions, overcoming challenges presented in the absorbance measurements of graphene oxide reduction assays.

This work compares image analysis of bacterial graphene oxide reduction with more traditional absorption measurement collection with a microplate reader. The digital image analysis avoids increased variance from graphene oxide flocculate settling and overlap between the bacteria and the graphene oxide absorbance spectra. These features result in increased resolution of the digital image analysis, enabling earlier detection of reduction activity as well as increased statistically significant differences between different sample types. This new method creates the opportunity for a model assay for *S. oneidensis* reduction reactions that emulates interactions between the organism and nanoparticles or bulk conductive substrates. The application of this technique as a model assay could improve the speed of microbial fuel cell optimization for fuel cells containing bulk substrates or nanoparticles, accelerating the rate of advancement in this field.

EXPERIMENTAL METHODS

Bacterial strains and culturing

S. oneidensis MR-1 (ATCC® 700550™) cultures were grown from freezer stocks stored in 25% glycerol at -80 ºC. Lysogeny broth (LB) media was prepared by dissolving tryptone (0.14 M, Sigma-Aldrich), yeast extract (15 mM, Sigma-Aldrich) and NaCl (0.17 M, Sigma-Aldrich) in de-ionised water. This solution was autoclaved for 30 minutes on a fluid cycle at 121 ºC and stored at room temperature. Frozen bacterial cultures were streaked onto LB-agar plates and incubated at 30 ºC overnight. The following day, a single colony was isolated and grown in LB (5 mL) at 30 ºC overnight under continuous shaking (200 rpm). These overnight cultures were used for graphene oxide reduction experiments.

Graphene oxide reduction assay

A solution of Minimal media was prepared as in Edwards, Jelusic, Kosko, McClelland, Ngarnim, Chiang, Lampa-Pastirk, Krauss, and Bren (2023)[70]; details are presented in SI Tables 1-4. To this solution, graphene oxide (0.12 g / L) was added. This solution was divided into 20 mL aliquots in individual 40 mL Environmental Protection Agency (EPA) vials (Sigma-Aldrich 23188). DL-lactic acid (10 mM, lactic acid) was added to some samples as an electron donor[37]. All samples were adjusted to pH 7 with 10 M sodium hydroxide. Nitrogen gas was bubbled though each vial for 10 minutes to create anaerobic conditions, which promotes increased lactate consumption by the *S. oneidensis*[30]. Overnight cultures of *S. oneidensis* prepared as described above were added to each vial at a 1:100 dilution, with three vials lacking bacteria to serve as a negative control. The samples were incubated at 30 ºC under continuous shaking (200 rpm).

Graphene oxide reduction assay comparing different bacteria optical densities

A frozen culture of *S. oneidensis* was streaked onto an LB-agar plate then grown overnight at 30 ºC. A single colony was isolated and grown in LB media at 30 ºC under continuous shaking (200 rpm). The optical density ($O.D._{600}$) of the culture was measured hourly using a Thermo Fisher Scientific™ Nanodrop to observe the absorbance of the solution at a wavelength of 600 nm. When the culture reached exponential growth phase (at an $O.D._{600}$ of 0.5), the bacterial culture was diluted to achieve variable $O.D._{600}$ values and was added to graphene oxide (0.12 g/L) in LB that had been flushed with nitrogen for 10 minutes to achieve anaerobic conditions.

Generation of plate reader and image data

At specific time points, the samples prepared above were placed in a light box to reduce interference from changing lighting and background and imaged with a Google© Pixel phone. RAW image files were used for analysis to avoid any interference from the imaging software.

RAW image files were converted to JPEG files using Adobe Lightroom© with no editing. The JPEG images were used for image analysis in MATLAB©.

Immediately after imaging, 100 µL aliquots were taken from each sample. The aliquots were placed into a 96 well plate, and their optical absorbance at 610 nm was measured using a Biotek© Synergy H1 microplate reader. These concurrent measurements enabled direct comparison between the measurements of graphene oxide reduction by digital image analysis and plate reader absorbance measurements of the same samples.

Color analysis of graphene oxide reduction sample images

The JPEG images obtained of graphene oxide reduction samples were subjected to further image analysis to obtain the average of the HSV value vector of each sample at different time-points. A workflow of the analysis procedure is presented in Figure 1. Analysis code was written in-house in MATLAB© and is available in the SI. For each image, the sample was selected and cropped to select an area that had minimal interference from background or reflections (Figure 1A). The orientation, location, focus, and selected area were kept consistent between images within an experiment. Within the selected area, at least 12 points were selected, avoiding any regions featuring reflections (Figure 1B). Around each point, a 32 x 32 pixel box was generated. The color data was represented by the HSV color space, which contains the color information of the selected crop box with three vectors[46] (Figure 1C). The H vector contains hue information: the color of each pixel. The S vector contains saturation information: how intense each pixel is. The V vector contains value information: how light or dark each pixel is. The HSV color space is advantageous over other color spaces for image analysis, such as the more typical RGB, because the data obtained is more stable under changing lighting conditions[47]. The value vector was isolated, and the average value was taken over the entire box. Each pixel was represented by a number between 0 and 1, where 0 is the darkest and 1 is

the lightest. This average value was calculated for each selected point, and the average overall value across all the points was determined to obtain an average across each sample. This method allowed for determination of the standard deviation over the sample for the analyzed points.

Image analysis of different graphene oxide concentrations

To determine the correlation of the value vector with the concentration of graphene oxide, different percentages of graphene oxide were mixed with LB media. Graphene oxide percentages ranged from 0.1% - 100%. Images were taken of the different samples in a lightbox, and the images were analysed digitally as described in the previous section. Average HSV vectors of the samples were compared to observe whether higher concentrations of graphene oxide corresponded to higher vector measurements.

Statistical analysis of data trends

Analysis was performed using Graphpad Prism™ to obtain p-values. An ANOVA test was performed with a Welch's correction to obtain the statistical difference between different sample trends.

Bootstrapping analysis was performed following the methods of B. Efron & R. Tibshirani (1993)[52,71]. Let $x_1, \dots, x_n$ be a sample distribution from a distribution with mean $\bar{x}$ and variance σ_x^2. Let $y_1, \dots, y_n$ be an independent sample distribution with mean $\bar{y}$ and variance σ_y^2. Then the test statistic is calculated as:

$$t = \frac{\bar{x} - \bar{y}}{\sqrt{\left(\frac{\sigma_x^2}{n}\right) + \left(\frac{\sigma_y^2}{n}\right)}}$$

Then create two new data sets where the values are $x_i' = x_i - \bar{x} + \bar{z}$ and $y_i' = y_i - \bar{y} + \bar{z}$, where $\bar{z}$ is the mean of the combined sample. Draw a random sample (x_i^*) of size n points from this pooled sample with replacement from x_i'. Draw another random sample (y_i^*) of size m points from this pooled sample with replacement from y_i'. Then calculate the test statistic:

$$t^* = \frac{\overline{x^*} - \overline{y^*}}{\sqrt{\left(\frac{\sigma_x^{*2}}{n}\right) + \left(\frac{\sigma_y^{*2}}{m}\right)}}$$

Repeat this algorithm 1,000,000 times (B = 100000) to estimate the p-value as:

$$p = \frac{\sum_0^B I\{t^* \geq t\}}{B}$$

Where $I\{t^* \geq t\}$ =1 when the condition is true. This method is advantageous for estimating the p-value from smaller datasets[52].

ACKNOWLEDGEMENTS

The authors wish to thank Professor Todd Krauss and Professor Kara Bren for initial discussions concerning the spectroscopy of the graphene oxide flocculates. The authors also wish to thank Dr. Elio Abbondanzieri for advice regarding bootstrapping analysis. Funding to D.B. and A.S.M. was provided by the Department of Energy via DE-SC0023354.

REFERENCES

(1) Harris, H. W.; El-Naggar, M. Y.; Nealson, K. H. Shewanella Oneidensis MR-1 Chemotaxis Proteins and Electron-Transport Chain Components Essential for Congregation near Insoluble Electron Acceptors. *Biochem. Soc. Trans.* **2012**, *40* (6), 1167–1177. https://doi.org/10.1042/BST20120232.

(2) Edwards, E. H.; Jelusic, J.; Kosko, R. M.; McClelland, K. P.; Ngarnim, S. S.; Chiang, W.; Lampa-Pastirk, S.; Krauss, T. D.; Bren, K. L. Shewanella Oneidensis MR-1 Respires CdSe Quantum Dots for Photocatalytic Hydrogen Evolution. *PNAS* **2023**, *120*, 17. https://doi.org/10.1073/pnas.

(3) El-Naggar, M. Y.; Wanger, G.; Leung, K. M.; Yuzvinsky, T. D.; Southam, G.; Yang, J.; Lau, W. M.; Nealson, K. H.; Gorby, Y. A. Electrical Transport along Bacterial Nanowires from Shewanella Oneidensis MR-1. *Proc. Natl. Acad. Sci. U. S. A.* **2010**, *107* (42), 18127–18131. https://doi.org/10.1073/pnas.1004880107.

(4) Rabaey, K.; Verstraete, W. Microbial Fuel Cells: Novel Biotechnology for Energy Generation. *Trends Biotechnol.* **2005**, *23* (6), 291–298. https://doi.org/10.1016/j.tibtech.2005.04.008.

(5) Rabaey, K.; Lissens, G.; Siciliano, S. D.; Verstraete, W. A Microbial Fuel Cell Capable of Converting Glucose to Electricity at High Rate and Efficiency. *Biotechnol. Lett.* **2003**, *25* (18), 1531–1535. https://doi.org/10.1023/A:1025484009367.

(6) Tao, M.; Jin, C.; Lu, H.; Jin, K.; Yu, L.; Liu, J.; Zhang, J.; Zhu, X.; Wu, Y. Living and Regenerative Material Encapsulating Self-Assembled Shewanella Oneidensis-CdS Hybrids for Photocatalytic Biodegradation of Organic Dyes. *Microorganisms* **2022**, *10* (12). https://doi.org/10.3390/microorganisms10122501.

(7) Cai, P. J.; Xiao, X.; He, Y. R.; Li, W. W.; Chu, J.; Wu, C.; He, M. X.; Zhang, Z.; Sheng, G. P.; Lam, M. H. W.; Xu, F.; Yu, H. Q. Anaerobic Biodecolorization Mechanism of Methyl Orange by Shewanella Oneidensis MR-1. *Appl. Microbiol. Biotechnol.* **2012**, *93* (4), 1769–1776. https://doi.org/10.1007/s00253-011-3508-8.

(8) Li, Q.; Feng, X.; Lu, X.; Li, T.; Han, X.; Xiao, X.; Wu, X.; Liu, Z.; Yang, M.; Feng, Y.

Combined Intra- and Extracellular Reduction Involved in the Anaerobic Biodecolorization of Cationic Azo Dye by Shewanella Oneidensis MR-1. *Chemosphere* **2018**, *211*, 701–708. https://doi.org/10.1016/j.chemosphere.2018.08.006.

(9) Zhang, X.; Epifanio, M.; Marsili, E. Electrochemical Characteristics of Shewanella Loihica on Carbon Nanotubes-Modified Graphite Surfaces. *Electrochim. Acta* **2013**, *102*, 252–258. https://doi.org/10.1016/j.electacta.2013.04.039.

(10) Gorby, Y. A.; Yanina, S.; McLean, J. S.; Rosso, K. M.; Moyles, D.; Dohnalkova, A.; Beveridge, T. J.; Chang, I. S.; Kim, B. H.; Kim, K. S.; Culley, D. E.; Reed, S. B.; Romine, M. F.; Saffarini, D. A.; Hill, E. A.; Shi, L.; Elias, D. A.; Kennedy, D. W.; Pinchuk, G.; Watanabe, K.; Ishii, S.; Logan, B.; Nealson, K. H.; Fredrickson, J. K. Electrically Conductive Bacterial Nanowires Produced by Shewanella Oneidensis Strain MR-1 and Other Microorganisms. *Proc. Natl. Acad. Sci. U. S. A.* **2006**, *103* (30), 11358–11363. https://doi.org/10.1073/pnas.0604517103.

(11) Lehner, B. A. E.; Janssen, V. A. E. C.; Spiesz, E. M.; Benz, D.; Brouns, S. J. J.; Meyer, A. S.; van der Zant, H. S. J. Creation of Conductive Graphene Materials by Bacterial Reduction Using Shewanella Oneidensis. *ChemistryOpen* **2019**, *8* (7), 888–895. https://doi.org/10.1002/open.201900186.

(12) Ford, K. C.; TerAvest, M. A. The Electron Transport Chain of Shewanella Oneidensis MR-1 Can Operate Bidirectionally to Enable Microbial Electrosynthesis. *Appl. Environ. Microbiol.* **2024**, *90* (1). https://doi.org/10.1128/aem.01387-23.

(13) Liu, W.; Liu, L.; Liu, C.; Hao, Y.; Yang, H.; Yuan, B.; Jiang, J. Methylene Blue Enhances the Anaerobic Decolorization and Detoxication of Azo Dye by Shewanella

Onediensis MR-1. *Biochem. Eng. J.* **2016**, *110*, 115–124. https://doi.org/10.1016/j.bej.2016.02.012.

(14) Torres, C. I.; Krajmalnik-Brown, R.; Parameswaran, P.; Marcus, A. K.; Wanger, G.; Gorby, Y. A.; Rittmann, B. E. Selecting Anode-Respiring Bacteria Based on Anode Potential: Phylogenetic, Electrochemical, and Microscopic Characterization. *Environ. Sci. Technol.* **2009**, *43* (24), 9519–9524. https://doi.org/10.1021/es902165y.

(15) Jiao, Y.; Qian, F.; Li, Y.; Wang, G.; Saltikov, C. W.; Gralnick, J. A. Deciphering the Electron Transport Pathway for Graphene Oxide Reduction by Shewanella Oneidensis MR-1. *J. Bacteriol.* **2011**, *193* (14), 3662–3665. https://doi.org/10.1128/JB.00201-11.

(16) Kotloski, N. J.; Gralnick, J. A. Flavin Electron Shuttles Dominate Extracellular Electron Transfer by Shewanella Oneidensis. **2013**, *4* (1), 10–13. https://doi.org/10.1128/mBio.00553-12.Editor.

(17) Pirbadian, S.; Barchinger, S. E.; Leung, K. M.; Byun, H. S.; Jangir, Y.; Bouhenni, R. A.; Reed, S. B.; Romine, M. F.; Saffarini, D. A.; Shi, L.; Gorby, Y. A.; Golbeck, J. H.; El-Naggar, M. Y. Shewanella Oneidensis MR-1 Nanowires Are Outer Membrane and Periplasmic Extensions of the Extracellular Electron Transport Components. *Proc. Natl. Acad. Sci. U. S. A.* **2014**, *111* (35), 12883–12888. https://doi.org/10.1073/pnas.1410551111.

(18) Subramanian, P.; Pirbadian, S.; El-Naggar, M. Y.; Jensen, G. J. Ultrastructure of Shewanella Oneidensis MR-1 Nanowires Revealed by Electron Cryotomography. *Proc. Natl. Acad. Sci. U. S. A.* **2018**, *115* (14), E3246–E3255. https://doi.org/10.1073/pnas.1718810115.

(19) Harris, H. W.; Sánchez-Andrea, I.; McLean, J. S.; Salas, E. C.; Tran, W.; El-Naggar,

M. Y.; Nealson, K. H. Redox Sensing within the Genus Shewanella. *Front. Microbiol.* **2018**, *8* (JAN), 1–11. https://doi.org/10.3389/fmicb.2017.02568.

(20) Beliaev, A. S.; Saffarini, D. A.; McLaughlin, J. L.; Hunnicutt, D. MtrC, an Outer Membrane Decahaem c Cytochrome Required for Metal Reduction in Shewanella Putrefaciens MR-1. *Mol. Microbiol.* **2001**, *39* (3), 722–730. https://doi.org/10.1046/j.1365-2958.2001.02257.x.

(21) Wu, C.; Cheng, Y. Y.; Li, B. B.; Li, W. W.; Li, D. B.; Yu, H. Q. Electron Acceptor Dependence of Electron Shuttle Secretion and Extracellular Electron Transfer by Shewanella Oneidensis MR-1. *Bioresour. Technol.* **2013**, *136*, 711–714. https://doi.org/10.1016/j.biortech.2013.02.072.

(22) Dong, Z.; Guo, S.; Fu, H.; Gao, H. Investigation of a Spontaneous Mutant Reveals Novel Features of Iron Uptake in Shewanella Oneidensis. *Sci. Rep.* **2017**, *7* (1), 1–12. https://doi.org/10.1038/s41598-017-11987-3.

(23) Wang, G.; Qian, F.; Saltikov, C. W.; Jiao, Y.; Li, Y. Microbial Reduction of Graphene Oxide by Shewanella. *Nano Res.* **2011**, *4* (6), 563–570. https://doi.org/10.1007/s12274-011-0112-2.

(24) Shi, L.; Squier, T. C.; Zachara, J. M.; Fredrickson, J. K. Respiration of Metal (Hydr)Oxides by Shewanella and Geobacter: A Key Role for Multihaem c-Type Cytochromes. *Mol. Microbiol.* **2007**, *65* (1), 12–20. https://doi.org/10.1111/j.1365-2958.2007.05783.x.

(25) McLean, J. S.; Pinchuk, G. E.; Geydebrekht, O. V.; Bilskis, C. L.; Zakrajsek, B. A.; Hill, E. A.; Saffarini, D. A.; Romine, M. F.; Gorby, Y. A.; Fredrickson, J. K.; Beliaev, A. S. Oxygen-Dependent Autoaggregation in Shewanella Oneidensis MR-1. *Environ.*

Microbiol. **2008**, *10* (7), 1861–1876. https://doi.org/10.1111/j.1462-2920.2008.01608.x.

(26) Brown, S. D.; Thompson, M. R.; VerBerkmoes, N. C.; Chourey, K.; Shah, M.; Zhou, J.; Hettich, R. L.; Thompson, D. K. Molecular Dynamics of the Shewanella Oneidensis Response to Chromate Stress. *Mol. Cell. Proteomics* **2006**, *5* (6), 1054–1071. https://doi.org/10.1074/mcp.M500394-MCP200.

(27) Breuer, M.; Rosso, K. M.; Blumberger, J.; Butt, J. N. Multi-Haem Cytochromes in Shewanella Oneidensis MR-1: Structures, Functions and Opportunities. *J. R. Soc. Interface* **2015**, *12* (102). https://doi.org/10.1098/rsif.2014.1117.

(28) Boas, J. V.; Oliveira, V. B.; Simões, M.; Pinto, A. M. F. R. Review on Microbial Fuel Cells Applications, Developments and Costs. *J. Environ. Manage.* **2022**, *307* (April 2021). https://doi.org/10.1016/j.jenvman.2022.114525.

(29) Logan, B. E.; Regan, J. M. Microbial Fuel Cells - Challenges and Applications. *Fuel Cells Technol. Fuel Process.* **2006**, No. 10, 1–32.

(30) Wang, H.; Correa, E.; Dunn, W. B.; Winder, C. L.; Goodacre, R.; Lloyd, J. R. Metabolomic Analyses Show That Electron Donor and Acceptor Ratios Control Anaerobic Electron Transfer Pathways in Shewanella Oneidensis. *Metabolomics* **2013**, *9* (3), 642–656. https://doi.org/10.1007/s11306-012-0488-3.

(31) Starwalt-Lee, R.; El-Naggar, M. Y.; Bond, D. R.; Gralnick, J. A. Electrolocation? The Evidence for Redox-Mediated Taxis in Shewanella Oneidensis. *Mol. Microbiol.* **2021**, *115* (6), 1069–1079. https://doi.org/10.1111/mmi.14647.

(32) Ntarlagiannis, D.; Atekwana, E. A.; Hill, E. A.; Gorby, Y. Microbial Nanowires: Is the Subsurface “Hardwired”? *Geophys. Res. Lett.* **2007**, *34* (17), 3–7.

https://doi.org/10.1029/2007GL030426.

(33) Coursolle, D.; Baron, D. B.; Bond, D. R.; Gralnick, J. A. The Mtr Respiratory Pathway Is Essential for Reducing Flavins and Electrodes in Shewanella Oneidensis. *J. Bacteriol.* **2010**, *192* (2), 467–474. https://doi.org/10.1128/JB.00925-09.

(34) Jin, X.; Wu, Y.; Peacock, C. L. .; Ashry, N. M.; Gao, C.; Huang, Q.; Cai, P. Outer Membrane C-Type Cytochromes OmcA and MtrC Play Distinct Roles in Enhancing the Attachment of Shewanella Oneidensis MR-1 Cells to Goethite. *Environ. Microbiol.* **2020**, *86* (23), 1–17.

(35) Roy, J. N.; Garcia, K. E.; Luckarift, H. R.; Falase, A.; Cornejo, J.; Babanova, S.; Schuler, A. J.; Johnson, G. R.; Atanassov, P. B. Applied Electrode Potential Leads to Shewanella Oneidensis MR-1 Biofilms Engaged in Direct Electron Transfer . *J. Electrochem. Soc.* **2013**, *160* (11), H866–H871. https://doi.org/10.1149/2.001401jes.

(36) Beliaev, A. S.; Klingeman, D. M.; Klappenbach, J. A.; Wu, L.; Romine, M. F.; Tiedje, J. M.; Nealson, K. H.; Fredrickson, J. K.; Zhou, J. Global Transcriptome Analysis of Shewanella Oneidensis MR-1 Exposed to Different Terminal Electron Acceptors. *J. Bacteriol.* **2005**, *187* (20), 7138–7145. https://doi.org/10.1128/JB.187.20.7138-7145.2005.

(37) Hong, Y.; Chen, X.; Guo, J.; Xu, Z.; Xu, M.; Sun, G. Effects of Electron Donors and Acceptors on Anaerobic Reduction of Azo Dyes by Shewanella Decolorationis S12. *Appl. Microbiol. Biotechnol.* **2007**, *74* (1), 230–238. https://doi.org/10.1007/s00253-006-0657-2.

(38) Voeikova, T. A.; Emel'yanova, L. K.; Novikova, L. M.; Mordkovich, N. N.; Shakulov, R. S.; Debabov, V. G. Mutants of an Electrogenic Bacterium Shewanella Oneidensis

MR-1 with Increased Reducing Activity. *Microbiol. (Russian Fed.* **2012**, *81* (3), 312–316. https://doi.org/10.1134/S0026261712030162.

(39) Bennett, B. D.; Brutinel, E. D.; Gralnick, J. A. A Ferrous Iron Exporter Mediates Iron Resistance in Shewanella Oneidensis MR-1. *Appl. Environ. Microbiol.* **2015**, *81* (22), 7938–7944. https://doi.org/10.1128/AEM.02835-15.

(40) Shih, C. J.; Lin, S.; Sharma, R.; Strano, M. S.; Blankschtein, D. Understanding the PH-Dependent Behavior of Graphene Oxide Aqueous Solutions: A Comparative Experimental and Molecular Dynamics Simulation Study. *Langmuir* **2012**, *28* (1), 235–241. https://doi.org/10.1021/la203607w.

(41) Gao, Y.; Zeng, X.; Zhang, W.; Zhou, L.; Xue, W.; Tang, M.; Sun, S. The Aggregation Behaviour and Mechanism of Commercial Graphene Oxide in Surface Aquatic Environments. *Sci. Total Environ.* **2022**, *806*, 150942. https://doi.org/10.1016/j.scitotenv.2021.150942.

(42) Fennessey, C. M.; Jones, M. E.; Taillefert, M.; Dichristina, T. J. Siderophores Are Not Involved in Fe(III) Solubilization during Anaerobic Fe(III) Respiration by Shewanella Oneidensis MR-1. *Appl. Environ. Microbiol.* **2010**, *76* (8), 2425–2432. https://doi.org/10.1128/AEM.03066-09.

(43) Huang, N. M.; Lim, H. N.; Chia, C. H.; Yarmo, M. A.; Muhamad, M. R. Simple Room-Temperature Preparation of High-Yield Large-Area Graphene Oxide. *Int. J. Nanomedicine* **2011**, *6*, 3443–3448. https://doi.org/10.2147/ijn.s26812.

(44) Cheng, X.; Dai, D.; Yuan, Z.; Peng, L.; He, Y.; Yeung, E. S. Color Difference Amplification between Gold Nanoparticles in Colorimetric Analysis with Actively Controlled Multiband Illumination. *Anal. Chem.* **2014**, *86* (15), 7584–7592.

https://doi.org/10.1021/ac501448w.

(45) Ouyang, M.; Di Carlo, D. Nanoplasmonic Swarm Biosensing Using Single Nanoparticle Colorimetry. *Biosens. Bioelectron.* **2019**, *132* (January), 162–170. https://doi.org/10.1016/j.bios.2019.02.056.

(46) Liu, Z.; Chen, W.; Zou, Y.; Hu, C. Regions of Interest Extraction Based on HSV Color Space. *IEEE Int. Conf. Ind. Informatics* **2012**, 481–485. https://doi.org/10.1109/INDIN.2012.6301214.

(47) Bennett, D.; Chen, X.; Walker, G. J.; Stelzer-Braid, S.; Rawlinson, W. D.; Hibbert, D. B.; Tilley, R. D.; Gooding, J. J. Machine Learning Color Feature Analysis of a High Throughput Nanoparticle Conjugate Sensing Assay. *Anal. Chem.* **2023**, *95* (16), 6550–6558. https://doi.org/10.1021/acs.analchem.2c05292.

(48) Bora, D. J.; Gupta, A. K.; Khan, F. A. Comparing the Performance of L*A*B* and HSV Color Spaces with Respect to Color Image Segmentation. *Int. J. Emerg. Technol. Adv. Eng.* **2015**, *5* (2), 192–203.

(49) Howell, D.; Rogier, M.; Yzerbyt, V.; Bestgen, Y. Statistical Methods in Human Sciences. *New York Wadsworth* **1998**.

(50) Hibbert, D. B.; Gooding, J. J. *Data Analysis for Chemistry*; Oxford University Press, 2005. https://doi.org/10.1093/oso/9780195162103.001.0001.

(51) Delacre, M.; Leys, C.; Mora, Y. L.; Lakens, D. Taking Parametric Assumptions Seriously: Arguments for the Use of Welch's f-Test Instead of the Classical f-Test in One-Way ANOVA. *Int. Rev. Soc. Psychol.* **2020**, *32* (1), 1–12. https://doi.org/10.5334/IRSP.198.

(52) Efron, B.; Tibshirani, R. *An Introduction to the Bootstrap*; Chapman & Hall, 1993; Vol. 23. https://doi.org/10.1111/1467-9639.00050.

(53) Wang, J.; Guo, X. The Gompertz Model and Its Applications in Microbial Growth and Bioproduction Kinetics: Past, Present and Future. *Biotechnol. Adv.* **2024**, *72* (February), 108335. https://doi.org/10.1016/j.biotechadv.2024.108335.

(54) Tjørve, K. M. C.; Tjørve, E. The Use of Gompertz Models in Growth Analyses, and New Gompertz-Model Approach: An Addition to the Unified-Richards Family. *PLoS One* **2017**, *12* (6), 1–17. https://doi.org/10.1371/journal.pone.0178691.

(55) Zwietering, M. H.; Jongenburger, I.; Rombouts, F. M.; Van't Riet, K. Modeling of the Bacterial Growth Curve. *Appl. Environ. Microbiol.* **1990**, *56* (6), 1875–1881. https://doi.org/10.1128/aem.56.6.1875-1881.1990.

(56) Alupoaei, C. E.; García-Rubio, L. H. Growth Behavior of Microorganisms Using UV-Vis Spectroscopy: Escherichia Coli. *Biotechnol. Bioeng.* **2004**, *86* (2), 163–167. https://doi.org/10.1002/bit.20001.

(57) Emiru, T. F.; Ayele, D. W. Controlled Synthesis, Characterization and Reduction of Graphene Oxide: A Convenient Method for Large Scale Production. *Egypt. J. Basic Appl. Sci.* **2017**, *4* (1), 74–79. https://doi.org/10.1016/j.ejbas.2016.11.002.

(58) Thompson, D. K.; Beliaev, A. S.; Giometti, C. S.; Tollaksen, S. L.; Khare, T.; Lies, D. P.; Nealson, K. H.; Lim, H.; Yates, J.; Brandt, C. C.; Tiedje, J. M.; Zhou, J. Transcriptional and Proteomic Analysis of a Ferric Uptake Regulator (Fur) Mutant of Shewanella Oneidensis: Possible Involvement of Fur in Energy Metabolism, Transcriptional Regulation, and Oxidative Stress. *Appl. Environ. Microbiol.* **2002**, *68* (2), 881–892. https://doi.org/10.1128/AEM.68.2.881-892.2002.

(59) Gabrielson, J.; Hart, M.; Jarelöv, A.; Kühn, I.; McKenzie, D.; Möllby, R. Evaluation of Redox Indicators and the Use of Digital Scanners and Spectrophotometer for Quantification of Microbial Growth in Microplates. *J. Microbiol. Methods* **2002**, *50* (1), 63–73. https://doi.org/10.1016/S0167-7012(02)00011-8.

(60) Uno, M.; Phansroy, N.; Aso, Y.; Ohara, H. Starch-Fueled Microbial Fuel Cells by Two-Step and Parallel Fermentation Using Shewanella Oneidensis MR-1 and Streptococcus Bovis 148. *J. Biosci. Bioeng.* **2017**, *124* (2), 189–194. https://doi.org/10.1016/j.jbiosc.2017.03.016.

(61) Pinchuk, G. E.; Geydebrekht, O. V.; Hill, E. A.; Reed, J. L.; Konopka, A. E.; Beliaev, A. S.; Fredrickson, J. K. Pyruvate and Lactate Metabolism by Shewanella Oneidensis MR-1 under Fermentation, Oxygen Limitation, and Fumarate Respiration Conditions. *Appl. Environ. Microbiol.* **2011**, *77* (23), 8234–8240. https://doi.org/10.1128/AEM.05382-11.

(62) Fitzgerald, L. A.; Petersen, E. R.; Gross, B. J.; Soto, C. M.; Ringeisen, B. R.; El-Naggar, M. Y.; Biffinger, J. C. Aggrandizing Power Output from Shewanella Oneidensis MR-1 Microbial Fuel Cells Using Calcium Chloride. *Biosens. Bioelectron.* **2012**, *31* (1), 492–498. https://doi.org/10.1016/j.bios.2011.11.024.

(63) Torres, C. I.; Marcus, A. K.; Rittmann, B. E. Proton Transport inside the Biofilm Limits Electrical Current Generation by Anode-Respiring Bacteria. *Biotechnol. Bioeng.* **2008**, *100* (5), 872–881. https://doi.org/10.1002/bit.21821.

(64) McCoy, T. M.; Pottage, M. J.; Tabor, R. F. Graphene Oxide-Stabilized Oil-in-Water Emulsions: PH-Controlled Dispersion and Flocculation. *J. Phys. Chem. C* **2014**, *118* (8), 4529–4535. https://doi.org/10.1021/jp500072a.

(65) Esmaeili, Y.; Bidram, E.; Zarrabi, A.; Amini, A.; Cheng, C. Graphene Oxide and Its Derivatives as Promising In-Vitro Bio-Imaging Platforms. **1993**, *10* (1), 1–13.

(66) Elias, D. A.; Tollaksen, S. L.; Kennedy, D. W.; Mottaz, H. M.; Giometti, C. S.; McLean, J. S.; Hill, E. A.; Pinchuk, G. E.; Lipton, M. S.; Fredrickson, J. K.; Gorby, Y. A. The Influence of Cultivation Methods on Shewanella Oneidensis Physiology and Proteome Expression. *Arch. Microbiol.* **2008**, *189* (4), 313–324. https://doi.org/10.1007/s00203-007-0321-y.

(67) Lies, D. P.; Hernandez, M. E.; Kappler, A.; Mielke, R. E.; Gralnick, J. A.; Newman, D. K. Shewanella Oneidensis MR-1 Uses Overlapping Pathways for Iron Reduction at a Distance and by Direct Contact under Conditions Relevant for Biofilms. *Appl. Environ. Microbiol.* **2005**, *71* (8), 4414–4426. https://doi.org/10.1128/AEM.71.8.4414-4426.2005.

(68) Mclean, J. S.; Wanger, G.; Gorby, Y. A.; Wainstein, M.; Mcquaid, J.; Ishii, S. I.; Bretschger, O.; Beyenal, H.; Nealson, K. H. Quantification of Electron Transfer Rates to a Solid Phase Electron Acceptor through the Stages of Biofilm Formation from Single Cells to Multicellular Communities. *Environ. Sci. Technol.* **2010**, *44* (7), 2721–2727. https://doi.org/10.1021/es903043p.

(69) Lu, M.; Chan, S.; Babanova, S.; Bretschger, O. Effect of Oxygen on the Per-cell Extracellular Electron Transfer Rate of Shewanella Oneidensis MR-1 Explored in Bioelectrochemical Systems. *Biotechnol. Bioeng.* **2017**, *114* (1), 96–105. https://doi.org/10.1002/bit.26046.

(70) Edwards, E. H. .; Jelusic, J.; Kosko, R. M. .; McClelland, K. P. .; Ngarnim, S. S. .; Chiang, W.; Lampa-Pastirk, S.; Krauss, T. D. .; Bren, K. L. Supplementary

Information for Shewanella Oneidensis MR-1 Respire CdSe Quantum Dots for Photocatalytic. *PNAS* **2023**, *120* (17), 1–30. https://doi.org/https://doi.org/10.1073/pnas.2206975120.

(71) Efron, B. Second Thoughts on the Bootstrap. *Stat. Sci.* **2003**, *18* (2), 135–140. https://doi.org/10.1214/ss/1063994968.